博士学位論文

新規リアルタイム可変型ボーラスの電子線治療への応用

近畿大学大学院
医学研究科医学系専攻
若林和樹

若林和樹

Doctoral Dissertation

A novel real-time shapeable soft rubber bolus for clinical use in electron radiotherapy

November 2022

Major in Medical Sciences
Kindai University Graduate School of Medical Sciences

Kazuki Wakabayashi

課博

同　意　書

2022年 11月 5日

近畿大学大学院
医学研究科長　殿

共著者 門前一 印　　共著者 田村 令 印

共著者 武井良樹 印　　共著者 奥畑勝也 印

共著者 阿南慎平 印　　共著者 土井啓至 印

共著者 西村恭昌 印　　共著者 ＿＿＿＿＿＿ 印

共著者 ＿＿＿＿＿＿ 印　　共著者 ＿＿＿＿＿＿ 印

論文題目

A novel real-time shapeable soft rubber bolus for clinical use in electron radiotherapy

下記の博士論文提出者が、標記論文を貴学医学博士の学位論文（主論文）として使用することに同意いたします。

また、標記論文を再び学位論文として使用しないことを誓約いたします。

記

1．博士論文提出者氏名　　若林　和樹

2．専攻分野　医学系　　医学物理学

近畿大学大学院医学研究科

A novel real-time shapeable soft rubber bolus for clinical use in electron radiotherapy

Kazuki Wakabayashi[1, 2], Hajime Monzen[1]*, Mikoto Tamura[1], Yoshiki Takei[1, 3], Katsuya Okuhata[1], Shimpei Anami[4], Hiroshi Doi[5], Yasumasa Nishimura[5].

[1] Department of Medical Physics, Graduate School of Medical Sciences, Kindai University, 377-2 Ohno-higashi, Osaka-Sayama, Osaka, 589-8511, Japan

[2] Department of Central Radiology, Wakayama Medical University Hospital, 811-1 Kimiidera, Wakayama, Wakayama, 641-8510, Japan

[3] Department of Radiology, Kindai University Nara Hospital, 1248-1 Otoda-cho, Ikoma, Nara 630-0293, Japan

[4] Department of Radiology, Wakayama Medical University, 811-1 Kimiidera, Wakayama, Wakayama, 641-8510, Japan

[5] Department of Radiation Oncology, Faculty of Medicine, Kindai University, 377-2 Ohno-higashi, Osaka-Sayama, Osaka 589-8511, Japan

*Corresponding author: Hajime Monzen, PhD

E-mail: hmon@med.kindai.ac.jp

Address: 377-2, Ohno-Higashi, Osaka-sayama, Osaka, 589-8511, Japan

Phone: +81. 72. 366. 0221

FAX: +81. 72. 368. 2388

Abstract

We have developed soft rubber (SR) bolus that can be shaped in real time by heating flexibly and repeatedly. This study investigated whether the SR bolus could be used as an ideal bolus, such as not changing of the beam quality and homogeneity through the bolus and high plasticity to adhere a patient in addition to real-time shapeable and reusability, in electron radiotherapy. Percentage depth doses (PDDs) and lateral dose profiles (LDPs) were obtained for 4, 6, and 9 MeV electron beams and were compared between the SR and conventional gel boluses. For the LDP at depth of 90% dose, the penumbra as lateral distance between the 80% and 20% isodose lines (P_{80-20}) and the width of 90% dose level (r_{90}) were compared. To evaluate adhesion, the air gap volume between the boluses and nose of a head phantom was evaluated on CT image. The dose profiles along the center axis for the 6 MeV electron beam with SR, gel, and virtual boluses (thickness = 5 mm) on the head phantom were also calculated for the irradiation of 200 monitor unit with a treatment planning system and the depth of the maximum dose (d_{max}) and maximum dose (D_{max}) were compared. The PDDs, P_{80-20}, and r_{90} between the SR and gel boluses corresponded well (within 2%, 0.4 mm, and 0.7 mm, respectively). The air gap volumes of the SR and gel boluses were 3.14 and 50.35 cm^3, respectively. The d_{max} with SR, gel and virtual boluses were 8.0, 6.0, and 7.0 mm (no-bolus: 12.0 mm), and the D_{max} values were 186.4, 170.6, and 186.8 cGy, respectively. The

SR bolus had the equivalent electron beam quality and homogeneity to the gel bolus and achieved excellent adhesion to a body surface, which can be used in electron radiotherapy as an ideal bolus.

Keywords: Real-time shapeable, Electron radiotherapy, Bolus, Soft rubber bolus

1. Introduction

Electron beams, which have a characteristic sharp drop off in dose beyond the tumor, are routinely applied to the treatment of skin, lip, head and neck cancers, the chest wall for breast cancer, keloid scars, and to boost doses to lymph nodes(Takei *et al* 2020, Khan and Gibbons 2014). For superficial tumors, a bolus can be used to increase the dose to the body surface(Kudchadker *et al* 2003, Khan and Gibbons 2014, Sharma *et al* 1983). Ideal bolus conditions are plasticity for high adhesion to a patient, shaping in real time, not changing of the beam quality and homogeneity through the bolus, and reusability. A vinyl gel sheet bolus (denoted as gel bolus), with the same absorptive and scattering properties as water or tissue-equivalent materials(White *et al* 1989), is widely used in clinical practice. However, it is difficult to adhere a gel bolus to non-flat surfaces such as head and neck tumors (e.g., nose, ear, and scalp(Hadziahmetovic *et al* 2014)) or the chest wall of post-mastectomy patients(Sharma and Johnson 1993); as a result, the bolus causes an unwanted air gap that decreases the dose to the skin(Sharma and Johnson 1993, Kong and Holloway 2007). A new patient-specific bolus created with 3D printing technology (denoted as 3D-printed bolus) has been developed(Park *et al* 2017, Kim *et al* 2014, Fujimoto *et al* 2017, Canters *et al* 2016, Ehler and Sterling 2020, Park *et al* 2016, Burleson *et al* 2015). The 3D-printed bolus improves adhesion to non-flat skin surfaces, reduces the air gap between the skin and bolus,

and prevents the dose decrease(Park *et al* 2019). The disadvantage of 3D-printed bolus is that the fabrication takes several hours to several days because of the need to obtain the patient's body surface data and the bolus cannot be reused.

At this time, we have developed a soft rubber (SR) bolus named the HM bolus (Hayakawa Rubber Co., Ltd., Hiroshima, Japan). The SR bolus can be shaped by hand when heated in real time and it maintains its shape at room and body temperatures, similar to a soft tungsten rubber(Monzen *et al* 2019, Matsumoto *et al* 2020, Kawai *et al* 2021, Wakabayashi *et al* 2021), thereby improving adhesion to the skin of various treatment sites. In this study, we investigated whether the SR bolus can be applied to electron radiotherapy as an ideal bolus.

2. Materials and Methods

2.1. Physical characteristics of the SR bolus

The SR bolus is a rubber material with no cross-linked polymerization, and it is a real-time variable-shaped material. The element ratios (wt%) of the SR bolus are H: 9.0%, C: 52.3%, O: 28.6%, Si: 10.0%, and other: 0.1%. The density was adjusted to 1.01 ± 0.03 g/cm^3 using silica as the reinforcement material. The resulting specific density was comparable to water (1.00 g/cm^3) and a conventional gel bolus (1.03 g/cm^3). The effective atomic number (Z_{eff}) was 8.07 (Khan and Gibbons 2014). The dynamic viscoelasticity of the SR bolus, assessed

by dynamic mechanical analysis(Geethamma *et al* 2005, Monzen *et al* 2019), is shown in Figure 1. The shape of the SR bolus was easily changed by hand (tan δ > 0.482 at 50℃), and its shape was maintained at lower temperature (tan δ < 0.37 at 40℃).

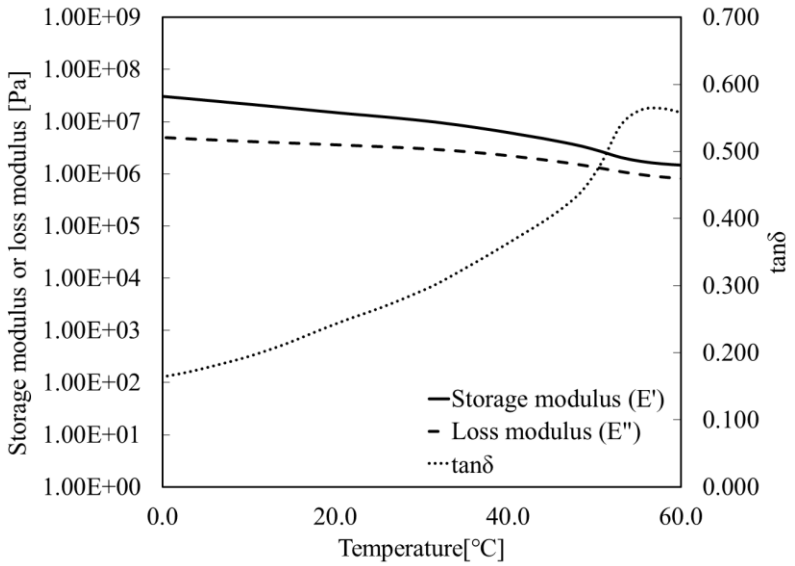

Figure 1. Dynamic viscoelasticity of the soft rubber (SR) bolus, assessed by dynamic mechanical analysis. The SR bolus had dimensions of 5.0 (W) × 45.0 (L) × 2.0 (T) mm^3, and the analysis was conducted at a frequency of 1.0 Hz(Najib *et al* 2011, Ivanova *et al* 2000) and an amplitude of 10 μm at 0–60℃ with a heating rate of 2℃/min using a DMS6100 system (Hitachi High-Tech Science Co., Tokyo Japan). The storage modulus (É) as elasticity, loss modulus (Ḗ) as viscosity, and the ratio of the moduli (Ḗ/É, defined as tan δ) are shown.

2.2. Dosimetric evaluation using the water-equivalent phantom

The dosimetric characteristics of the SR bolus with respect to the electron beams were evaluated by the percent depth doses (PDDs) and lateral dose profiles (LDPs) for 4, 6, and 9 MeV electron beams. The SR bolus was placed on a water-equivalent phantom (Tough Water Phantom; Kyoto Kagaku Co., Ltd. Kyoto, Japan), and the PDD and LDP at the depth of a 90% dose were obtained using a parallel-plate ionization chamber (Roos Type 34001; PTW, Freiburg, Germany), RAMTEC smart electrometer (Toyo Medic, Tokyo, Japan), and Gafchromic EBT3 film (ISP, Wayne, NJ, USA) (Figure 2). The EBT3 film was placed orthogonally to the beam axis (orthogonal plane) (Figure 2b). The PDD curves and LDPs were normalized to the maximum dose and central axis of the beam, respectively. The film dosimetry and calibration were treated as described in our previous work(Takei *et al* 2020). The PDDs and LDPs of the SR bolus were compared with those of a commercially available gel bolus (Bolx-I, CIVCO Medical Solution, Orange City, IA, USA) (density: 1.03 g/cm^3). The thicknesses of the SR bolus and gel bolus were both 5 and 10 mm, and their sizes were 25 cm × 25 cm and 30 cm × 30 cm, respectively. Electron beams with nominal energies of 4, 6, and 9 MeV from an Elekta Synergy linac (Elekta AB, Stockholm, Sweden) were used for all measurements. The electron applicator size was 10 cm × 10 cm at the source to surface distance (SSD) of 100 cm. A dose of 200 monitor units (MU) was irradiated.

For the PDD curves, the dosimetric characteristics of both boluses were compared with the following evaluation items;

1. d_{max}: depth of the maximum dose.

2. d_{90}: depth of 90% of the maximum dose.

3. d_{80}: depth of 80% of the maximum dose.

4. R_{80-20}: depth from the 80% and 20% isodose lines.

5. R_p: depth of the point where the tangent to the descending linear portion of the curve intersects the extrapolated background(Khan and Gibbons 2014).

6. D_x: photon contamination dose at the end of the electron range, determined from the tail of the depth dose curve by reading the dose value at the point where the curve becomes straight(Khan and Gibbons 2014).

R_{80-20}, R_p, and D_x represent the dose falloff, practical range, and photon contamination dose regions by the bremsstrahlung, respectively(Khan and Gibbons 2014).

For the LDPs at d_{90}, the distal side of the treatment area, the penumbra (as the lateral distance between the 80% and 20% isodose lines, P_{80-20}), and the width of the 90% dose area (r_{90}) relative to the beam central axis dose were evaluated.

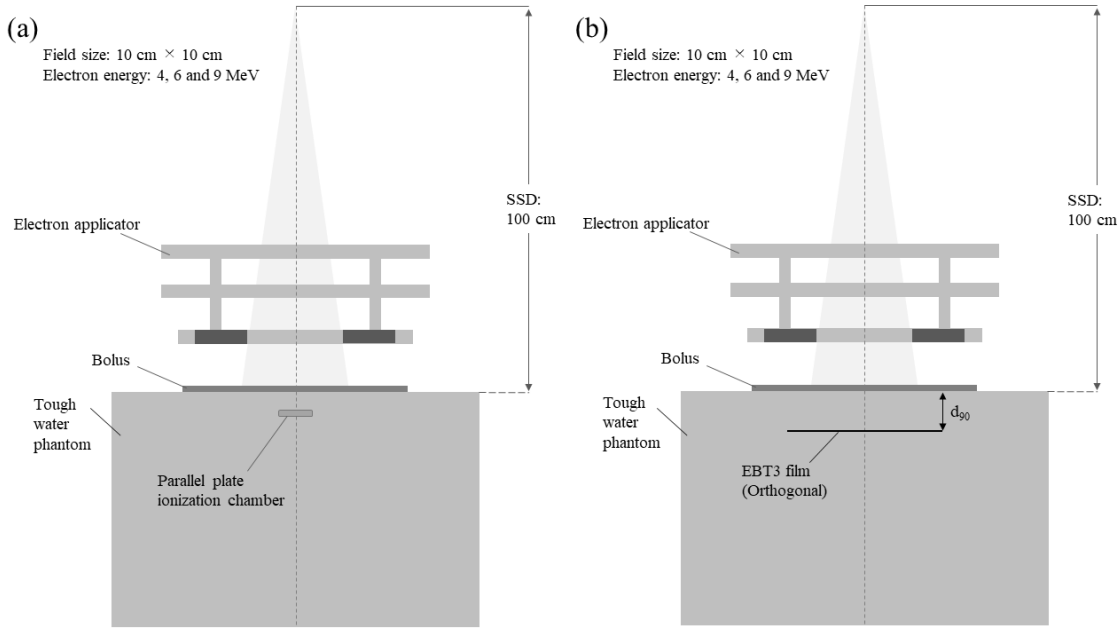

Figure 2. Schematics of the experimental geometries for (a) percentage depth doses and (b) lateral dose profiles. SSD: source to surface distance.

2.3. Evaluation of the adhesion of the SR bolus

The adhesion of the SR bolus to the body surface was evaluated according to the air gap volume between the phantom surface and bolus at the nose of an anthropomorphic head phantom (PBU-1, Kyoto Kagaku Co., Ltd., Kyoto, Japan). A 5-mm-thick SR bolus with an area of 15 cm × 15 cm wrapped in clingfilm was heated at 500 W for 3 min in a microwave oven and then lightly pressed against the nose of the phantom. A 5-mm-thick gel bolus with an area of 30 cm × 30 cm was also placed in the same position and CT images were obtained for each bolus using an Acquilion LB CT system (Canon Medical Systems, Tochigi, Japan).

The imaging conditions were as follows: tube voltage = 120 kV, tube current = 300 mA, matrix size = 512 × 512 pixels, field of view = 500 mm, and slice thickness = 2 mm. The air gap volume was calculated by manual contouring of the air gap between the phantom and bolus in an area 6.4 cm from the nasal apex to the nasal root of the CT image using a treatment planning system (Pinnacle^3: Philips Medical Systems, Andover, MA, USA).

2.4. Comparison of dose distributions in treatment planning system

To assess the use of the SR bolus in clinical practice, the dose distribution of a nasal virtual skin tumor in a head phantom using the SR bolus was compared with that without bolus, with gel bolus, and with virtual bolus(Fujimoto *et al* 2017). The same CT images in Section *2.3* were used. The virtual bolus was created by expanding the head phantom surface by 5 mm, and the density was set to 1.00 g/cm^3. The virtual target was delineated below the phantom surface with a thickness of 1.0 cm and a virtual target volume of 16.9 cm^3. The gantry angle, field size, electron beam energy, and irradiated MU were set to 30°, 6 cm × 6 cm, 6 MeV, and 200 MU, respectively. The dose calculation algorithm implemented on the Pinnacle^3 system was the Collapsed Cones Convolution Superposition algorithm, and the dose calculation grid size was set to 2 mm × 2 mm × 2 mm. The dose profiles along the beam center axis were obtained for the SR bolus, no bolus, gel bolus, and virtual bolus

conditions. The d_{max}, phantom surface dose (D_{0mm}), depth of 5 mm dose (D_{5mm}), and maximum dose (D_{max}) from the dose profiles were compared between each bolus.

3. Results

3.1. Dosimetric evaluation using the water-equivalent phantom

Figure 3 shows the PDD curves for the SR bolus and gel bolus. The d_{max}, d_{90}, d_{80}, R_{80-20}, R_p, and D_x values are shown in Table 1. The PDDs of the SR bolus were in close agreement with those of the gel bolus. The differences in PDD values between the SR bolus and gel bolus were within 2%, except for a difference of 2.8% at depth of 15 mm for the 5-mm bolus and a difference of 2.7% at depth = 9 mm for the 10-mm bolus with the 4 MeV electron beam. The d_{max}, d_{90}, d_{80}, R_{80-20}, and R_p values were consistent to within 0.5 mm for each energy and bolus thickness of the SR bolus and gel bolus. The photon contamination dose was 0.4, 0.8, and 1.3% for both the SR bolus and gel bolus with the 4, 6, and 9 MeV electron beams, respectively. The P_{80-20} and r_{90} values from the LDPs (Table 2) were consistent within 0.4 mm and 0.7 mm, respectively.

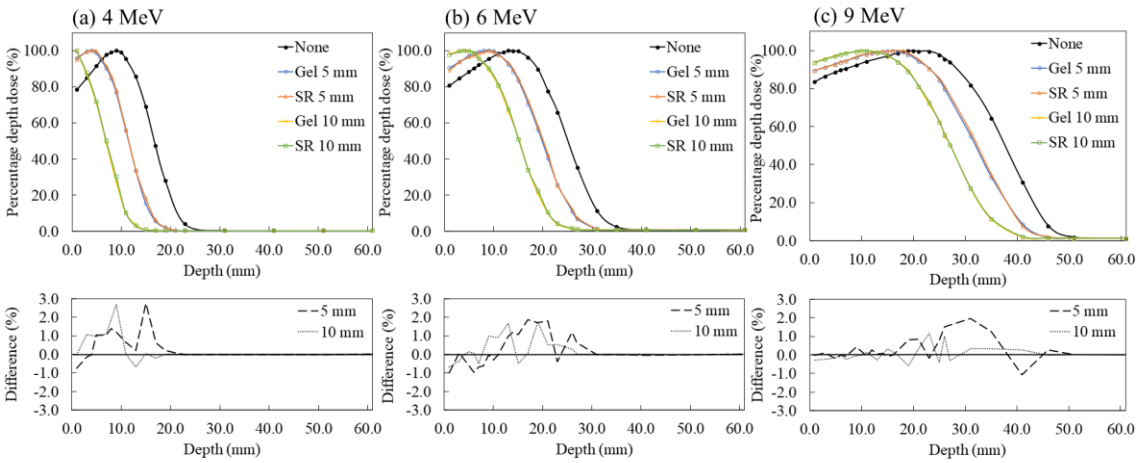

Figure 3. Percent depth dose curves (top) and percent differences between soft rubber (SR) bolus and gel bolus (bottom) for (a) 4, (b) 6, and (c) 9 MeV electron beams. SR: SR bolus. Gel: gel bolus.

Table 1. Dosimetric characteristics of the percent depth dose curves with no bolus, soft rubber (SR) bolus, and gel bolus.

Energy		No-bolus	Bolus thickness			
			5 mm		10 mm	
			SR bolus	Gel bolus	SR bolus	Gel bolus
4 MeV	d_{max} (mm)	9.0	4.0	4.0	1.0	1.0
	d_{90} (mm)	12.1	7.3	7.1	2.7	2.5
	d_{80} (mm)	13.7	8.8	8.6	4.0	3.9
	R_{80-20} (mm)	6.7	6.0	5.9	6.0	6.0
	R_p (mm)	20.5	14.9	14.9	11.4	11.4
	D_x (%)	0.4	0.4	0.4	0.4	0.4
6 MeV	d_{max} (mm)	13.0	9.0	9.0	4.0	4.0
	d_{90} (mm)	18.9	13.9	13.6	9.0	8.8
	d_{80} (mm)	20.6	15.7	15.5	11.1	11.0
	R_{80-20} (mm)	8.9	8.4	8.6	8.3	8.1
	R_p (mm)	30.6	25.3	25.1	19.5	20.0
	D_x (%)	0.8	0.8	0.8	0.8	0.8
9 MeV	d_{max} (mm)	20.0	16.0	16.0	10.0	10.0
	d_{90} (mm)	28.3	23.1	23.2	18.6	18.8
	d_{80} (mm)	31.4	26.3	25.9	21.3	21.2
	R_{80-20} (mm)	11.9	12.0	12.3	11.6	11.6
	R_p (mm)	45.4	40.0	39.9	34.7	34.4
	D_x (%)	1.3	1.3	1.3	1.3	1.3

Table 2. The penumbra value (P_{80-20}) and width of the 90% isodose line (r_{90}) from the lateral dose profile analysis at d_{90} with no bolus, soft rubber (SR) bolus, and gel bolus.

Energy		No-bolus	Bolus thickness			
			5 mm		10 mm	
			SR bolus	Gel bolus	SR bolus	Gel bolus
4 MeV	P_{80-20} (mm)	13.4	11.6	11.6	11.6	11.6
	r_{90} (mm)	81.8	83.8	83.9	81.8	82.5
6 MeV	P_{80-20} (mm)	13.0	12.7	12.7	12.3	12.3
	r_{90} (mm)	82.8	80.7	80.7	83.5	82.8
9 MeV	P_{80-20} (mm)	12.3	13.0	12.7	12.3	12.7
	r_{90} (mm)	78.9	76.9	76.2	76.5	76.2

3.2. Evaluation of the adhesion of the SR bolus

Figure 4 shows the CT images of the SR bolus and gel bolus placed on the head phantom. The SR bolus was shaped and set on the phantom within 20 s of heating in the microwave oven. The air gap volumes between the head phantom and the SR and gel boluses were 3.14 cm^3 and 50.35 cm^3, respectively.

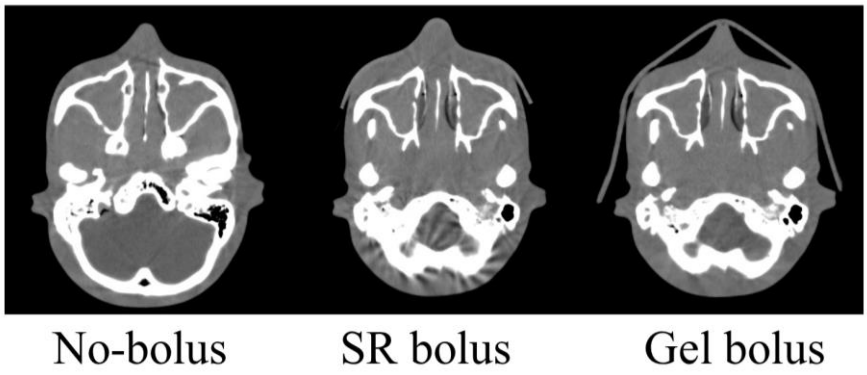

Figure 4. CT images with no bolus, soft rubber (SR) bolus, and gel bolus.

3.3. Comparison of dose distributions in treatment planning system

The dose distributions and dose profiles for the head phantom along the beam center axis are shown in Figs. 5 and 6, and the dosimetric parameters are shown in Table 3. The depth of 0.0 mm represents the phantom surface. The d_{max} values of the dose profiles with SR bolus, gel bolus, and virtual bolus were shifted by 4.0, 6.0, and 5.0 mm compared with the no bolus condition, respectively. The values of D_{0mm} were 159.8, 155.6, and 164.8 cGy for the SR bolus, gel bolus, and virtual bolus, respectively, and the values of D_{max} were 178.5, 186.4, 170.6, and 186.8 cGy for the no bolus, SR bolus, gel bolus, and virtual bolus, respectively. The value of D_{5mm} for no bolus, which was measured at the same depth (i.e., 0 mm) with the 5-mm bolus, was 159.6 cGy.

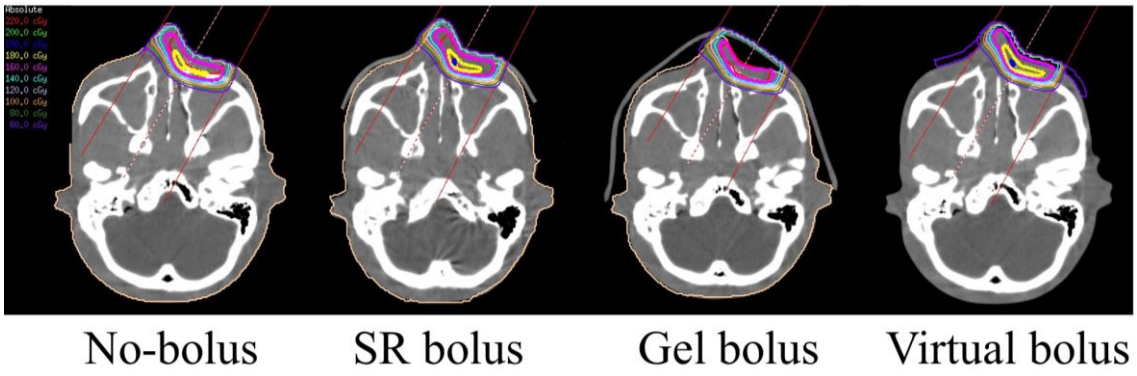

Figure 5. Dose distribution with no bolus, soft rubber (SR) bolus, gel bolus, and virtual bolus. Thickness of each bolus: 5 mm, Electron beam energy: 6 MeV, Irradiated dose: 200 monitor unit.

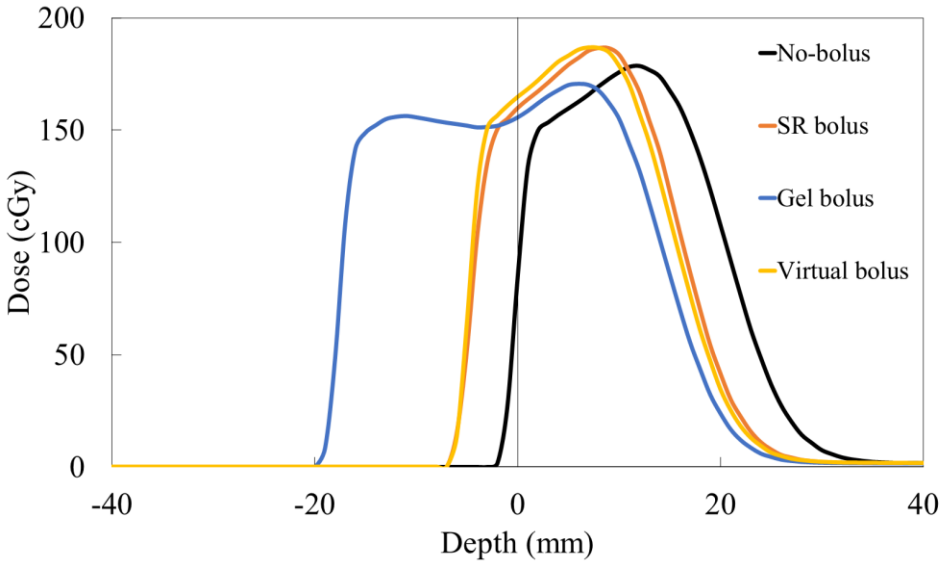

Figure 6. Dose profiles along the beam center axis for the head phantom. The depth of 0.0 mm represents the phantom surface. The thickness of both the soft rubber (SR) bolus and gel bolus was 5.0 mm.

Table 3. Dosimetric parameters of the dose profile along the beam center axis in the head phantom. The thickness of the soft rubber (SR) bolus, gel bolus, and virtual bolus was 5 mm.

	d_{max} (mm)	D_{0mm} (cGy)	D_{max} (cGy)
No-bolus	12.0	84.4	178.5
SR bolus	8.0	159.8	186.4
Gel bolus	6.0	155.6	170.6
Virtual bolus	7.0	164.8	186.8

4. Discussion

We developed a real-time shapeable SR bolus with a tissue-equivalent density that can be freely shaped at temperatures of >50℃ and maintains its shape at room and body

temperatures. The SR bolus had equivalent PDDs and LDPs to those of the gel bolus (Fig. 3 and Tables 1 and 2) and achieved excellent adhesion to non-flat body surfaces (Fig. 4). The SR bolus provides ideal bolus properties such as plasticity for high adhesion, shaping in real time, beam quality and homogeneity equivalent to gel bolus, and reusability.

The dose distribution in the water-equivalent phantom using the SR bolus corresponded well with that using the gel bolus (Fig. 3 and Tables 1 and 2). The density of the SR bolus was adjusted by the silica reinforcement material and had equivalent absorption and scattering properties to those of the gel bolus. In terms of the photon contamination dose, the SR bolus was comparable to no bolus and gel bolus, which indicates that the amount of bremsstrahlung generated by the SR bolus was same as that with no bolus or gel bolus(Khan and Gibbons 2014). Therefore, the electron beam quality was not changed when using the SR bolus.

The SR bolus sufficiently adhered to non-flat body surfaces even in areas where the air gap was a problem for the gel bolus (Fig. 4), and an equivalent bolus effect was observed without decreasing the skin dose to the phantom surface (Figs. 5 and 6). The SR bolus can be applied to all skin areas with and without non-flat superficial targets, such as skin, lips, head and neck, chest wall, lymph nodes, and keloid scars. The maximum air gap between the gel bolus and the phantom surface was approximately 2.0 cm (Fig. 5), which resulted in a maximum dose and skin dose reductions of 5.6% and 8.7% compared with the virtual bolus,

respectively (Table 3). Sharma et al. suggested that a skin dose reduction of approximately 10% might be caused by an air gap of 2.0 cm with a 5-mm bolus with a 6 cm × 6 cm irradiation field and a 6 MeV electron beam(Sharma and Johnson 1993). The setup of the gel bolus according to the CT simulation at each irradiation is also challenge, which causes a discrepancy between the planned dose and actual delivered dose(Fujimoto *et al* 2017, Khan and Gibbons 2014, Kim *et al* 2014). The SR bolus can be employed in CT simulation and treatment planning directly after shaping in real time (e.g., within 20 s of heating in a microwave oven) because the bolus has no metal artifacts and has a beam quality equivalent to a virtual bolus (Fig. 6 and Table 3). Therefore, the setup and planned dose can be realized using the SR bolus.

Aoyama et al. described a thermoset shape memory bolus made of poly-ε-caprolactone polymer was able to be shaped in real time without using a 3D printer, while the thickness of the shape-memory bolus is 1.5 mm, and it was difficult to make it thicker(Aoyama *et al* 2020). The shape and thickness of the SR bolus can be adjusted on demand clinically, such as shaping for each individual target. The SR bolus is expected to be applied to modulated electron radiotherapy that creates a dose distribution to fit the shape of the target for each patient(Zhao *et al* 2017), improving target dose coverage, and sparing organs-at-risk beyond the target. The SR bolus is also reusable with reheating (e.g., using 70°C water for 10 min)

after each treatment. The limitation of the SR bolus is that it hides the superficial target, although marking a line on the SR bolus may address this problem.

5. Conclusions

The SR bolus achieves excellent adhesion to the body surface by shaping in real time, can be reused, and has equivalent electron beam quality and homogeneity to a conventional gel bolus. The SR bolus can be used in electron radiotherapy as an ideal bolus.

Acknowledgement

This work was supported partly by Japan Society for the Promotion of Science (JSPS) KAKENHI grant number 19K08211 and 20K08093. Hajime Monzen received a research donation from Hayakawa Rubber Co., Ltd. We thank Richard Lipkin, PhD, and Ashleigh Cooper, PhD, from Edanz Group (https://jp.edanz.com/ac) for editing a draft of this manuscript.

References

Aoyama T, Uto K, Shimizu H, Ebara M, Kitagawa T, Tachibana H, Suzuki K and Kodaira T 2020 Physical and dosimetric characterization of thermoset shape memory bolus developed for radiotherapy *Med. Phys.* **47** 6103–12

Burleson S, Baker J, Hsia A T and Xu Z 2015 Use of 3D printers to create a patient-specific 3D bolus for external beam therapy *J. Appl. Clin. Med. Phys.* **16** 166–78

Canters R A, Lips I M, Wendling M, Kusters M, van Zeeland M, Gerritsen R M, Poortmans P and Verhoef C G 2016 Clinical implementation of 3D printing in the construction of patient specific bolus for electron beam radiotherapy for non-melanoma skin cancer *Radiother. Oncol.* **121** 148–53

Ehler E D and Sterling D A 2020 3D printed copper-plastic composite material for use as a radiotherapy bolus *Phys. Med.* **76** 202–6

Fujimoto K, Shiinoki T, Yuasa Y, Hanazawa H and Shibuya K 2017 Efficacy of patient-specific bolus created using three-dimensional printing technique in photon radiotherapy *Phys. Med.* **38** 1–9

Geethamma V G, Kalaprasad G, Groeninckx G and Thomas S 2005 Dynamic mechanical behavior of short coir fiber reinforced natural rubber composites *Compos. Part A Appl. Sci. Manuf.* **36** 1499–506

Hadziahmetovic M, Weldon M, Pearson M, Werner P and Siddiqui F 2014 Scalp uniform bolus application (SCUBA) technique for homogenous scalp and regional nodal irradiation *Pract. Radiat. Oncol.* **4** e95–9

Ivanova K I, Pethrick R A and Affrossman S 2000 Investigation of hydrothermal ageing of a filled rubber toughened epoxy resin using dynamic mechanical thermal analysis and dielectric spectroscopy *Polymer* **41** 6787–96

Kawai Y, Tamura M, Amano M, Kosugi T and Monzen H 2021 First clinical experience of tungsten rubber electron adaptive therapy with real-time variable-shape tungsten rubber *Anticancer Res.* **41** 919–25

Khan F M and Gibbons J P 2014 *Khan's The Physics of Radiation Therapy* (Philadelphia: LIPPINCOTT WILLIAMS & WILKINS/WOLTERS KLUWER)

Kim S W, Shin H J, Kay C S and Son S H 2014 A customized bolus produced using a 3-dimensional printer for radiotherapy *PLoS One* **9** e110746

Kong M and Holloway L 2007 An investigation of central axis depth dose distribution pertubation due to an air gap between patients and bolus for electron beams *Australas. Phys. Eng. Sci. Med.* **30** 111–9

Kudchadker R J, Antolak J A, Morrison W H, Wong P F and Hogstrom K R 2003 Utilization of custom electron bolus in head and neck radiotherapy *J. Appl. Clin. Med. Phys.* **4** 321–33

Matsumoto K, Tamura M, Otsuka M, Wakabayashi K, Kijima K and Monzen H 2020 Dosimetric characteristics of a real time shapeable tungsten containing rubber with electron beams *Nihon Hoshasen Gijutsu Gakkai Zasshi* **76** 1248–55

Monzen H, Tamura M, Kijima K, Otsuka M, Matsumoto K, Wakabayashi K, Choi M-G, Yoon D-K, Doi H, Akiyama H and Nishimura Y 2019 Estimation of radiation shielding ability in electron therapy and brachytherapy with real time variable shape tungsten rubber *Phys. Med.* **66** 29–35

Najib N N, Ariff Z M, Bakar A A and Sipaut C S 2011 Correlation between the acoustic and dynamic mechanical properties of natural rubber foam: Effect of foaming temperature *Mater. Des.* **32** 505–11

Park J M, Son J, An H J, Kim J H, Wu H G and Kim J I 2019 Bio-compatible patient-specific elastic bolus for clinical implementation *Phys. Med. Biol.* **64** 105006

Park K, Park S, Jeon M J, Choi J, Kim J W, Cho Y J, Jang W S, Keum Y S and Lee I J 2017 Clinical application of 3D-printed-step-bolus in post-total-mastectomy electron conformal therapy *Oncotarget* **8** 25660–8

Park S Y, Choi C H, Park J M, Chun M S, Han J H and Kim J I 2016 A patient-specific polylactic acid bolus made by a 3D printer for breast cancer radiation therapy *PLoS One* **11** e0168063

Sharma S C, Deibel F C and Khan F M 1983 Tissue equivalence of bolus materials for electron beams *Radiology* **146** 854–5

Sharma S C and Johnson M W 1993 Surface dose perturbation due to air gap between patient and bolus for electron beams *Med. Phys.* **20** 377–8

Takei Y, Kamomae T, Monzen H, Nakaya T, Sugita K, Suzuki K, Oguchi H, Tamura M and Nishimura Y 2020 Feasibility of using tungsten functional paper as a thin bolus for electron beam radiotherapy *Phys. Eng. Sci. Med.* **43** 1101–11

Wakabayashi K, Monzen H, Tamura M, Matsumoto K, Takei Y and Nishimura Y 2021 Dosimetric evaluation of skin collimation with tungsten rubber for electron radiotherapy: A Monte Carlo study *J. Appl. Clin. Med. Phys.* **22** 63–70

White D R, Booz J, Griffith R V., Spokas J J and Wilson I J 1989 ICRU Report 44: Tissue substitutes in radiation dosimetry and measurement. *J. Int. Comm. Radiat. Units Meas.* **23**

Zhao Y, Moran K, Yewondwossen M, Allan J, Clarke S, Rajaraman M, Wilke D, Joseph P and Robar J L 2017 Clinical applications of 3-dimensional printing in radiation therapy *Med. Dosim.* **42** 150–5